# Generalized Swept Mid-structure for Polygonal Models

Tobias Martin[†1], Guoning Chen[2], Suraj Musuvathy[1], Elaine Cohen[1] and Charles Hansen[1,2]

[1]School of Computing, University of Utah, USA
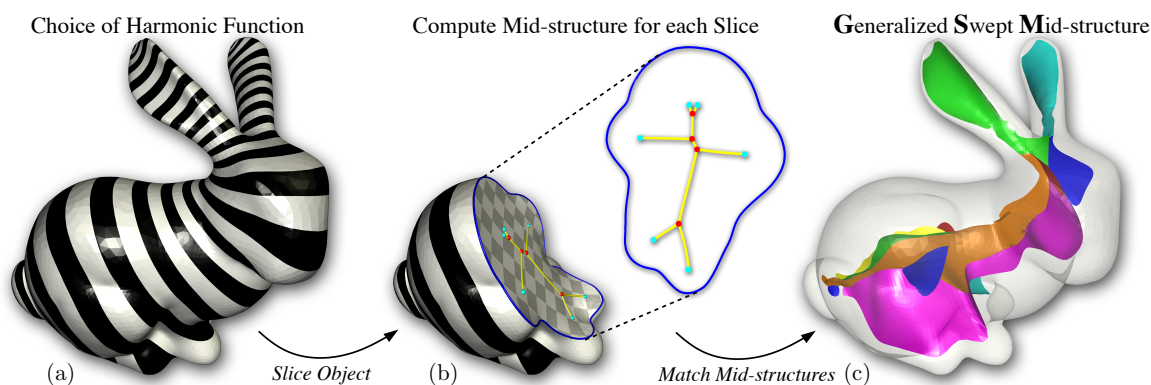[2]SCI, University of Utah, USA



**Figure 1:** *Pipeline for the Generalized Swept Mid-structure (GSM): (a) User choice of harmonic function. (b) Object is decomposed into (curved) slices, and a medial axis is computed for each slice. (c) Slices are iteratively matched into a GSM (colored surface sheets).*

**Abstract**
*We introduce a novel mid-structure called the generalized swept mid-structure (GSM) of a closed polygonal shape, and a framework to compute it. The GSM contains both curve and surface elements and has consistent sheet-by-sheet topology, versus triangle-by-triangle topology produced by other mid-structure methods. To obtain this structure, a harmonic function, defined on the volume that is enclosed by the surface, is used to decompose the volume into a set of slices. A technique for computing the 1D mid-structures of these slices is introduced. The mid-structures of adjacent slices are then iteratively matched through a boundary similarity computation and triangulated to form the GSM. This structure respects the topology of the input surface model is a hybrid mid-structure representation. The construction and topology of the GSM allows for local and global simplification, used in further applications such as parameterization, volumetric mesh generation and medical applications.*

## 1. Introduction

Many applications in the field of computer graphics and visualization require interior mid-structures of three dimensional objects that represent their form or shape with lower dimensional entities. One dimensional curve skeletons [ATC*08], and the 3D medial axis [SP08], are such examples that have

been used for mesh generation, animation, registration, and segmentation applications. Curve skeletons faithfully represent an object in tubular regions. For more general geometry, a medial axis is preferred since it consists of surface sheets [SP08] and they better capture the shape than curve skeletons.

However, a medial axis is very sensitive to small changes in shape and it produces nearly degenerate polygons in tubular regions. Our quest for a new type of mid-structure is moti-
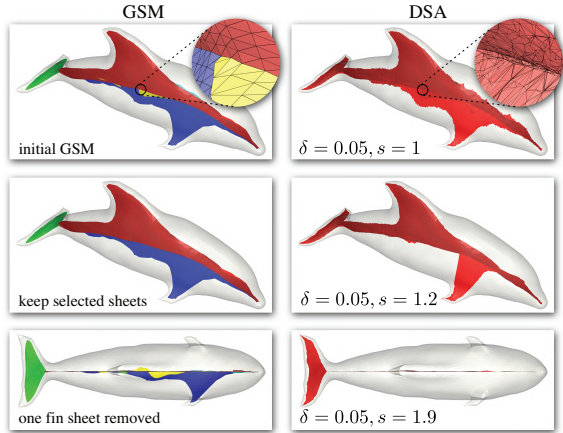
---

[†] martin@cs.utah.edu

**Figure 2:** *Sheet based simplification using GSM (left) vs. global simplification using DSA (right). Magnified regions compare triangulations in a region where surfaces meet. Only the GSM shows 3 distinct sheets (red, blue, yellow) while the DSA shows similar polygons. The yellow GSM sheet (top left) is removed (mid left GSM). To simplify DSA in this region requires removal of additional structures in other regions (mid right DSA). Bottom row illustrates removal of a large blue sheet on one side of the GSM, whereas simplification of the DSA results in removal of polygons from both sides.*



**Figure 3:** *The tight co-cone is intrinsic to the object, consisting of accurate but complex medial topology. A GSM identifies sheets (blue, red and white) and because of its swept generation, it has a natural parameterization.*

vated by three reasons. (1) In some situations, it is desirable for a user to design a skeleton. Since a user might be aware of which regions require higher fidelity elements and a reduced number of extraordinary points in later simulations, the user can design a midstructure to yield the appropriate mesh layout. This is similar to the motivation of the approach presented in [MCK08] and [MC10] and is difficult to achieve with medial axis computation algorithms. (2) The topological structure and connectivity information of mid-structure components is often required for the aforementioned applications. However, existing techniques for medial axis computation of polygonal models (e.g. tight co-cone [DG03], powercrust [ACK01], discrete scale axis (DSA) [MGP10]) do not classify surface sheets of the medial axis as illustrated in the magnified view in Figure 2. Given a polygonal medial axis representation, identifying surface sheets requires post-processing that often includes topological fixing and establishing connectivity information. This is a tedious process as it requires extensive human input. (3) Neither curve skeletons nor 3D medial axes have an embedded parameterization (see Figure 3). Such a parameterization can be useful for 3D cross field design [NRP11, HTWB11].

This paper introduces the *Generalized Swept Mid-structure* (GSM) (Figure 1) with the three properties:
**(1)** The GSM is a hybrid mid-structure consisting of both curve and surface elements, that is suitable for an input shape consisting of both general and tubular regions (e.g., hand model in Figure 8).
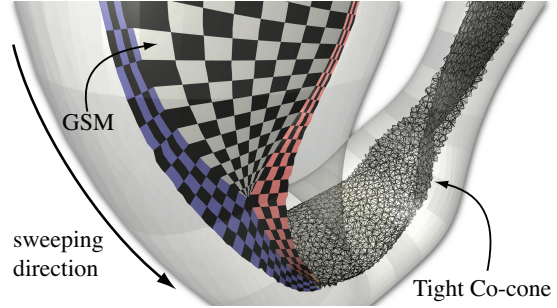
**(2)** Analogously to [HXS09] for curve skeletons or [NGH04] in computing fair morse functions to extract the topological structure of a surface mesh, the user determines a sweeping strategy by choosing a harmonic function that conforms naturally to an object's shape. Apart from this specification, the construction of the GSM is automatic. From this harmonic function a 3D harmonic function is computed. In this work, mid-structures (i.e. simplified medial axes) of level sets of the 3D harmonic function are swept across the input object (Figure 1 (a) and (b)) to generate a GSM. The level sets are typically non-planar regions. This generality reduces the number of connected components and therefore enables the approach to be used for a wide variety of objects. A theoretical framework for a swept medial axis was proposed in [Dam08]. The goal of that work was to present theoretical results on geometric properties of the object in terms of medial axes of the planar slices. In our work, we present practical algorithms for an implementation of a generalization of that framework and demonstrate several results.

**(3)** The swept nature of a GSM suggests a parameterization strategy. Namely, one parameter is assigned as the harmonic function value and the second parameter is obtained by assigning parameter values to the mid-structure of each slice. Figure 3 shows an example. Furthermore, the GSM construction approach automatically classifies the various sheets of the mid-structure, computed by tracking transitions of curve segments of the mid-structures of the level sets. Given the sheet-by-sheet topology of the GSM (see colored sheets in Figure 1 c), the user can select sheets of the GSM that are to be preserved or removed in a simplification procedure (see Figure 2). A simplified mid-structure can be used in subsequent applications, such as generation of 3D cross fields or volumetric parameterization.

The contributions of this paper include: **1.** Introduction of the GSM, a novel mid-structure based on sweeps of mid-structures of non-planar level sets, and a pipeline to compute it (Section 3). **2.** A novel planar medial axis computation algorithm, from which the mid-structure is computed (Section 5).

**3.** A matching algorithm for consecutive mid-structures to create a GSM with consistent topology (Section 6).

## 2. Related Work

There have been vast research on mid-structures related to the proposed GSM. 1D curve skeletons and 3D medial axes are special types of mid-structures. Algorithms for computing them are reviewed in the surveys [SP08, BAB*08].

In a similar fashion to the GSM construction, level set diagrams [LV99] are constructed by connecting barycenters of isocontours of a scalar function defined on a surface. Curve skeletons are extracted by improving Reeb graphs of harmonic functions in [HXS09]. Mesh contraction using constrained Laplacian smoothing is used to construct curve skeletons in [ATC*08].

Exact arithmetic is used to compute medial axes of polyhedra in [CKM04]. Approximations of the medial axis of polygonal meshes are computed using distance fields in [FLM03] and Voronoi diagrams in [SFM05]. Algorithms for computing medial axes from point-sampled surfaces based on Voronoi graphs are [ACK01, DG03, CL04]. The discrete scale axis [MGP10] is a variant of the medial axis that computes connected polygons of medial surfaces corresponding to dominant shape features at a user specified simplification scale.

Voronoi based medial axis computation algorithms are computationally efficient. However, since there is no sheet topology information, there is no explicit relationship between medial axis regions and object shape features. Furthermore, in contrast to a GSM, global methods do not suggest a strategy to parameterize the resulting medial axis, at least in part because sheet structure is undetermined. With an explicit sweeping direction, the GSM identifies sheets, and has a natural parameterization that can be used for later applications as discussed in Section 8. Figure 3 shows a comparison between the tight co-cone and GSM.

A hybrid structure is derived via topological analysis of the 3D medial axis of an object in [GDB06] and is used to annotate tubular and more general regions of the object. However, the derived structure is susceptible to problems associated with medial axis computation. Thinning algorithms such as those presented in [JBC07] are used to derive skeletons of objects represented as sub-regions of volumetric grid data. The derived skeletons consist of discrete voxels without topology. The topology must be inferred in a post process, and is susceptible to errors stemming from sampling density and object orientation within the grid. Our proposed approach automatically generates curve and surface sheet skeletons in appropriate areas with consistent topology at the transition regions and sheet topology in surface regions.

## 3. The GSM

The generalized swept mid-structure (GSM) is a mid-structure obtained by joining mid-structures of nonplanar slices of a polygonal representation of a closed 3D object. The GSM, a connected structure lying in the interior of the object, is a generalization of the swept medial axis as proposed in [Dam08]. The GSM consists of triangulated surfaces and curves represented as polylines. The GSM is invariant under rigid body transformations and scaling.

### 3.1. Computational Pipeline Overview

This section provides an overview of our methodology to construct a mid-structure for a closed surface triangle mesh. Let $(\mathcal{T}, \mathcal{V}_T, \mathcal{C}_T)$ define the bounding triangle mesh, where $\mathcal{T}$ is the set of triangles, $\mathcal{V}_T$ is the set of vertices, and $\mathcal{C}_T$ is the connectivity of the mesh. Based on $\mathcal{T}$, a volumetric representation $\Omega \subset \mathbb{R}^3$ is constructed, represented as an unstructured tetrahedral mesh, denoted by $(\mathcal{H}, \mathcal{V}_H, \mathcal{C}_H)$, where $\mathcal{H} \subset \mathbb{R}^3$ is the set of tetrahedra, $\mathcal{V}_H$ the set of vertices defining the tetrahedra, and $\mathcal{C}_H$ the connectivity of the tetrahedral mesh. $\mathcal{H}$ is constructed using a tetrahedral meshing method, e.g. [Si05], and has $\mathcal{T}$ as its boundary.

The following steps describe the construction of GSM from the input shape $\mathcal{T}$, as shown in Figure 1,

1. Compute a harmonic function $u(x,y,z)$ on $\mathcal{H}$ (Section 4).

2. Decompose $\mathcal{H}$ into a sequence of non-planar slices $L_i$ ($L_i$ are level sets of $u(x,y,z)$) (Section 4.1).

3. Extract a simplified 2D mid-structure for each $L_i$ (Section 5).

4. Starting from the first slice, iteratively construct the mid-structure by matching the mid-structures of two adjacent slices until the last slice is reached (Section 6).

## 4. Harmonic Functions

The GSM framework can be used if the dataset already contains a slicing strategy (e.g. segmented data from a volumetric scan). In this case we proceed to step 2 in the GSM construction pipeline. Otherwise, we compute a harmonic function.

A harmonic function is a function $u \in C^2(\mathcal{H}), u : \mathcal{H} \to \mathbb{R}$, satisfying Laplace's equation,

$$\nabla^2 u = 0, \qquad (1)$$

where $\nabla^2 = \partial^2/\partial x_1^2 + \partial^2/\partial x_2^2 + \partial^2/\partial x_3^2$. $u$ satisfies the maximum principle, i.e. it does not exhibit any local minima and maxima, and therefore can be used to define a sweeping strategy to decompose $\mathcal{H}$ into an ordered set of slices. Harmonic functions have been used earlier in the domain of meshing and volumetric parameterization [DKG05, MCK08] or for skeleton extraction [HXS09].

Galerkin's formulation [Hug00] is used to discretize Equation 1. $\mathcal{V}_H$ can be decomposed into the set $\mathcal{V}_B$ for which the solution is known (Dirichlet boundary) and the set $\mathcal{V}_I$, for which a solution is sought. A solution has the form
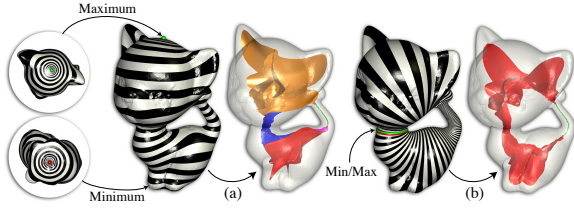
**Figure 4:** *Two different harmonic functions on kitten model result in different GSMs.*

$u(x,y,z) = \sum_{\mathbf{v} \in \mathcal{V}} \hat{u}_k \phi_k(x,y,z)$, where $\phi_k(x,y,z)$ are linear hat functions associated with vertex $v_k \in \mathcal{V}$. The gradient field $\nabla u$ over $\mathcal{H}$ is therefore piecewise constant.

In our framework, many methods can be used to create the slicing strategy, such as [DBG*06], but we chose approaches similar to [NGH04, DKG05, HXS09], where the user determines the points in the set $\mathcal{V}_B$. The user therefore has control over $u(x,y,z)$ and the resulting sweeping strategy. Figure 4 illustrates two harmonic functions on the genus-1 kitten model. While $u(x,y,z)$ in Figure 4a has two saddles, $u(x,y,z)$ in Figure 4b follows a torus-like sweep. Both are valid, Figure 4 also shows the corresponding GSMs for these two distinct choices.

### 4.1. Decomposition of $\mathcal{H}$

Given the harmonic function $u(x,y,z)$, a slice $L_i$ (Figure 1b), at value $u_i \in \mathbb{R}$ is the level set satisfying $u(x,y,z) = u_i$. $L_i$ is extracted using marching tetrahedra [CFM*94]. Depending on the choice of $\mathcal{V}_B$ and resulting saddle points [NGH04], $L_i$ can consist of multiple disjoint non-planar 2-manifolds represented with triangle meshes with boundaries.

Once the user specifies the harmonic function $u(x,y,z)$, which determines the cutting strategy, the object is decomposed into a set of slices $L_i$ such that every triangle in $\mathcal{T}$ is intersected by at least one slice which captures the global features in $\mathcal{T}$. For each vertex $p_i^k$ of $L_i$, a path can be constructed from $p_i^k$ to a new point $p_j^k$, the *projection* of $p_i^k$ on level set $L_j$, by following $\nabla u(x,y,z)$. Let $l_{i,j}^k$ be the length of this path.

Then, given this set of slices, let $\varepsilon_i = \max_{\forall k} \{l_{i,i+1}^k\}$ be the distance between slice $i$ and $i+1$. Due to distortions of $u(x,y,z)$ and triangulation of $\mathcal{T}$, $\varepsilon_i$ varies across the slices. To achieve a cutting of the object such that $\varepsilon_i$ varies slowly, the input surface is remeshed into a triangle mesh where triangles have approximately the same size and shape. These parameters can be chosen by the user to maintain a specific feature size. Such a triangulation can be computed using, for instance, Afront [SSS06]. Section 7 presents an example that shows GSMs of different versions of an input object.

Each component of $L_i$ is flattened using the CGAL [cga] implementation of the LSCM [LPRMt02]. The boundary of the flattened $L_i$ is approximated with a periodic B-spline

curve using the method proposed in [MCK08]. A medial axis with topological structure is computed for the planar region enclosed by this curve, using a novel technique presented in Section 5. This medial axis is simplified, yielding the mid-structure which is mapped onto the respective component of $L_i$ and incrementally matched with that of an adjacent slice to construct the GSM (Section 6).

## 5. Computing Mid-structure of Slices

In order to construct reliable GSMs, we require mid-structures to consist of smooth curves and smoothly changing geometry and topology between adjacent slices. Several techniques for computing the medial axis of a planar region from piecewise smooth [RG03, AAA*09] or discrete boundary representations [SP08, BAB*08] exist. However, such approaches introduce artifacts, due to the nature of the representation, and human interaction is required to remove them to compute a suitable mid-structure. We present a new method to automatically and accurately compute the medial axis with topology of the parametric B-spline curve that approximates the boundary of the flattened level set $L_i$. A suitable mid-structure is then computed by simplifying the medial axis based on its topology.

The medial axis of a planar region enclosed by a bounding curve $\gamma$ is the locus of centers of maximally inscribed circles that are tangent to two points on $\gamma$, with the limit points of the locus [GK03]. The contact points of each maximal circle with the boundary curve are called *foot points* for the corresponding medial axis point. A limit point is either an *end point* or a *junction point* at which the maximally inscribed circle has one or three foot points, respectively. Three medial curve segments meet at a junction point. Figure 5 shows an example of the medial axis of a planar region computed using our proposed approach. Our approach also computes foot points and distance to the boundary for each medial axis point, thereby giving the complete medial axis transform. Foot points, end points and junction points are not explicitly produced in previous medial axis computation algorithms. These points are necessary for the matching stage proposed in Section 6.

### 5.1. Algorithm Overview

The proposed approach is based on the eikonal flow (also called grassfire flow) of the boundary curve toward the interior. Let $\mathcal{B}$ be the boundary of a region in $\mathbb{R}^2$ represented by a parametric B-spline curve $\gamma(u)$. The inward directed curve normal is defined as $N(u,v) = [0\ 0\ 1]^T \times \frac{\partial \gamma(u)}{\partial u}$, which avoids flips of normal vector directions at inflection points. The offset curve resulting from the eikonal flow at a time $t$ is given by $\mathcal{C}(u,t) = \gamma(u) + t \frac{N(u)}{\|N(u)\|}, t \geq 0$. As the curve evolves under the eikonal flow, different regions start intersecting with each other at distinct points, and the intersection points evolve as $t$ increases. The trace of each such point is the medial axis. Note that only the first intersection points of any two

boundary points belong to the medial axis. The eikonal flow results in the occurrence of two kinds of transition points: 1) source points, at which medial curves are created, and 2) sink points, at which medial curves are annihilated. The proposed approach presents techniques to accurately compute all transition points using properties of the B-spline representation. Medial curves are then computed using a numerical tracing algorithm. This topology structure and connectivity is required in the mid-structure matching stage, to establish consistent topology for the GSM.

## 5.2. Transition Points

We present geometric criteria for computing transition points, where the resulting nonlinear B-spline equations are solved using state-of-the-art methods [EK01, EG08] that guarantee robust computation of all solutions where accuracy is chosen to be $1/10$ of the current slicing distance $\varepsilon_i$, using their implementation in the IRIT library [Elb08]. Let $\gamma_i(u_i)$, $i = 1, 2, 3$ be three representations of the boundary curve to denote different regions, and let $N_i$ denote the unnormalized normals of $\gamma_i$ respectively that are directed toward the interior of the region of interest.

**End points** are source points of the medial axis corresponding to curvature maximum points of $\gamma(u)$. The parameter values of critical points of curvature ($\kappa(u)$) are computed by solving Equation 2. End points are those solutions that correspond to maximum values of $\kappa$, and are computed at offset $\frac{1}{\kappa}$.

$$\frac{\partial \kappa(u)}{\partial u} = \frac{\partial}{\partial u}\left(\frac{\|\frac{\partial \gamma}{\partial u} \times \frac{\partial^2 \gamma}{\partial u^2}\|}{\|\frac{\partial \gamma}{\partial u}\|^3}\right) = 0 \qquad (2)$$

**Distance critical points** are points where the distance between two points on $\gamma$ corresponding to a medial axis point is a critical value. The critical point is a source point when the distance function has a local minimum, and a sink point when the distance function has a local maximum. Define $\mathcal{D}(u_1, u_2) = \|\gamma_1 - \gamma_2\|^2 = \langle \gamma_1 - \gamma_2, \gamma_1 - \gamma_2 \rangle$ as the squared distance function between any two points on the curve. The parameter values corresponding to critical points of $\mathcal{D}$ are obtained by computing solutions of Equation 3. Distance critical points are given by $(\gamma(u_1) + \gamma(u_2))/2$.

$$\frac{\partial \mathcal{D}}{\partial u_i} = \langle \gamma_1 - \gamma_2, \frac{\partial \gamma_i}{\partial u_i} \rangle = 0, \ i = 1, 2 \qquad (3)$$

A **junction point** is either a sink point for three curves or a sink for two curves and a source for a third one [GK03]. For a point $P \in \mathbb{R}^2$ to be a junction point, the following equations must be satisfied.

$$\langle P - \gamma_i, \frac{\partial \gamma_i}{\partial u_i} \rangle = 0, \ i = 1, 2, 3 \qquad (4a)$$

$$\| P - \gamma_1 \| = \| P - \gamma_j \|, \ j = 2, 3 \qquad (4b)$$

Since $P = (x, y)$ is unknown, Equations 4(a)-(b) form a system of five equations in five unknowns. This system is simplified in a way similar to that in [EK01]. Let $P = \gamma_1 + \alpha N_1$.
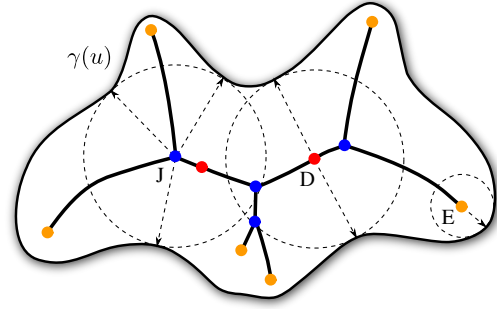


**Figure 5:** *Medial axis of a region bounded by a B-spline curve. Along with their maximal circles, end points (E) are shown in orange, junction points (J) in blue, and distance critical points (D) in red. The arrows point to the foot points.*

Substitute for $P$ in $\| P - \gamma_1 \| = \| P - \gamma_2 \|$, to obtain $\alpha = \frac{-\langle \gamma_1 - \gamma_2, \gamma_1 - \gamma_2 \rangle}{2\langle \gamma_1 - \gamma_2, N_1 \rangle}$. Denote $\gamma_1 - \gamma_i$ by $\gamma_{1mi}, i = 2, 3$. Substituting for $P$ and $\alpha$ in Equations 4(a)-(b) and simplifying yields a system of 3 equations in 3 variables. For $i = 2, 3$,

$$2\langle \gamma_{1m2}, N_1 \rangle \langle \gamma_{1mi}, \frac{\partial \gamma_i}{\partial u_i} \rangle - \| \gamma_{1m2} \|^2 \langle N_1, \frac{\partial \gamma_i}{\partial u_i} \rangle = 0 \qquad (5a)$$

$$\langle \gamma_{1m2}, N_1 \rangle \| \gamma_{1m3} \|^2 - \| \gamma_{1m2} \|^2 \langle N_1, \gamma_{1m3} \rangle = 0 \qquad (5b)$$

Equation 4(a) for $i = 1$ is automatically satisfied after substitutions for $P$ and $\alpha$. From the corresponding parameter values and solutions, junction points are computed as offsets at distance given by $\alpha \| N(u_1) \|$. Among all solutions of Equations 3 and 5, only those that satisfy the maximality condition are retained. Trivial solutions where $u_l = u_m, l \neq m$ are ignored.

## 5.3. Medial Curves

Suppose $\mathcal{C}_i$, $i = 1, 2$ are two representations of eikonal offset curves of $\gamma_i(u_i)$ at time $t$. Define a mapping $F : \mathbb{R}^3_{u_1, u_2, t} \to \mathbb{R}^2$, where $\mathbb{R}^3_{u_1, u_2, t}$ is the augmented parameter space consisting of the parametric directions of the two curves and the time domain, as follows

$$F(u_1, u_2, t) = \mathcal{C}_1(u_1, t) - \mathcal{C}_2(u_2, t), u_1 \neq u_2 \qquad (6)$$

The parametric domain, $\mathcal{I}$, of $F(u_1, u_2, t) = [0\ 0]^T$ is the set of all intersection points of the two offset curves over all time values. Away from transition points, $F$ is a differentiable function, and hence $\mathcal{I}$ is a well-defined 1-manifold in $\mathbb{R}^3_{u_1, u_2, t}$. Let $F^{(x)}$ and $F^{(y)}$ represent the first and second vector components of $F$. $\mathcal{I}$ is an implicit space curve that is the locus of intersection points of the two hypersurfaces $F^{(x)} = 0$ and $F^{(y)} = 0$. The tangent to the intersection curve $\mathcal{I}$ is given by

$$T_{\mathcal{I}} = \nabla F^{(x)} \times \nabla F^{(y)} \qquad (7)$$

where $\nabla F^{(x)}$ and $\nabla F^{(y)}$ are the normals to the hypersurfaces. The medial axis curve segments are numerically traced from source ($P_{SRC}$) to sink points in the augmented parameter space by solving the differential equation (Equation 8).

$$\frac{d\chi}{dt} = T_{\mathcal{I}}(\chi), \quad \chi(0) = P_{SRC}, \quad \chi(t) \in \mathbb{R}^3_{u_1, u_2, t} \quad (8)$$

Sink points are detected during numerical tracing when they are within a specified distance. This distance is a percentage of the diagonal of bounding box of $\gamma$. For the results shown in this paper, a distance tolerance of 1% worked well.

### 5.4. Medial Axis Simplification

The mid-structure is constructed by simplifying the computed medial axis. Leaf segments are deleted and internal segments are merged. Medial segments incident at distance critical points are merged. These operations are performed when the respective segment length is smaller than the slicing distance ($\varepsilon_i$). Note that this procedure may result in more than three incident curves at a junction point, but does not add complexity to the matching algorithm presented in the next section.

If all segments of the medial axis are smaller than $\varepsilon_i$, the medial axis is contracted to the centroid of the region. This situation occurs when the boundary is nearly circular and therefore the medial axis consists of small segments near the center of the region. These contractions result in 1D curve segments in the GSM. We will denote a topological graph of the mid-structure of the level set $L_i$ as $M_i = G(N_i, E_i)$, where $N_i$ is the set of the end points and junction points, and $E_i$ is the set of edges that connect these points. These edges correspond to the curved segments in the original mid-structures that are densely sampled for later GSM representation. $p_i^j$ is used to denote the $j^{th}$ node in $N_i$, and $(p_i^j, p_i^k) \in E_i$ represents the edge between those nodes .

## 6. Matching Successive 2D Mid-Structure

After computing mid-structures for each level set (Section 5), we next find correspondence between two neighboring 2D mid-structures and construct a surface to connect them. Given the two successive mid-structures represented as two graphs (Section 5), we match the edges of the graphs. A triangulation is used to connect these matching pairs based on the samples along the original mid-structure (see figure below). A number of existing graph matching techniques can be applied to accomplish this step [GT91,SSDZ98,KSK01]. However, these methods typically deal with more general



graph matching problems without knowing the relation between the two graphs that are matched. Thus, their algorithms are usually complicated and computationally expensive. In contrast, in the present problem, one graph is evolved from
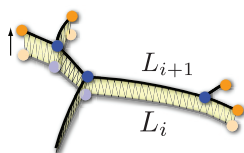
the other through a small change and hence the generic transitions between the two graphs are well-defined [GK03]. Therefore, a simpler matching technique can be devised by finding the correspondences along the section boundary curves from which the mid-structures are computed (Section 5).

### 6.1. Topological Changes

For smoothly changing geometry of the boundary, there are only two generic transitions of the mid-structures [GK03]: **Leaf creation/annihilation (*Type 1*)** and **Flip configuration (*Type 2*)**. *Type 1* corresponds to the creation (or destruction) of a feature (e.g. a protrusion) on the boundary. To illustrate *Type 2*, consider the junction points, $p_i^j$ and $p_i^k$ in $M_i$ and $p_{i+1}^l$ and $p_{i+1}^r$ in $M_{i+1}$, respectively. Each pair is connected by an edge. In the continuous case, edge $(p_i^j, p_i^k)$ will first collapse into a single node before growing to edge $(p_{i+1}^l, p_{i+1}^r)$. However, the discrete cutting will



likely not capture the degenerate point as shown in the figure to the right.
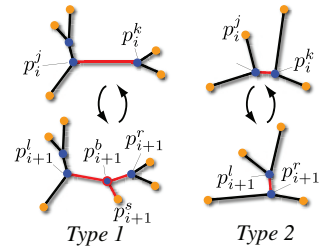
During matching, we assume at most one topoligical change on an edge (including its two end points) of the graph when evolving from one level set to the next. If this assumption is not satisfied, additional level sets between the original pair must be added until it is satisfied. Other cases are investigated in a future work.

### 6.2. Matching

Let $\{cp_i\}$ be the set of foot points of $M_i$. We match two graphs $M_i$ and $M_{i+1}$ according to the distance of $\{cp_i\}$ and $\{cp_{i+1}\}$ on $\partial L_{i+1}$. We first *project* $\{cp_i\}$ (on $\partial L_i$) to $\partial L_{i+1}$ as discussed in Section 4.1. On the boundary of the level set $L_{i+1}$, the distance between any two foot points $cp$ and $cp'$ is defined as the shortest arc-length between them along $\partial L_{i+1}$, $\widehat{(cp, cp')}$. Assume that all foot points are sorted along $\partial L_{i+1}$ (either clockwise or counter clockwise). Given a foot point $cp_i^j$ of $M_i$, there are exactly two points $cp_{i+1}^l$ and $cp_{i+1}^r$ from $M_{i+1}$ that enclose $cp_i^j$ along the 1D boundary $\partial L_{i+1}$. Therefore, finding the closest point to a given foot point can be done in constant time. Two end points $p_i^j$, $p_{i+1}^r$ (Figure 6, bottom left) from the two graphs are called *close* if their foot points are the closest pair on $\partial L_{i+1}$. We then pair them in the matching, denoted as $p_i^j \leftrightarrow p_{i+1}^r$. Two junction points $p_i^g$, $p_{i+1}^b$ (Figure 6, middle left) from the two graphs are called *close* if the foot points of $p_i^g$ are directly next to the ones of $p_{i+1}^b$ pairwisely on $\partial L_{i+1}$ or their leaf nodes are all close to each other.

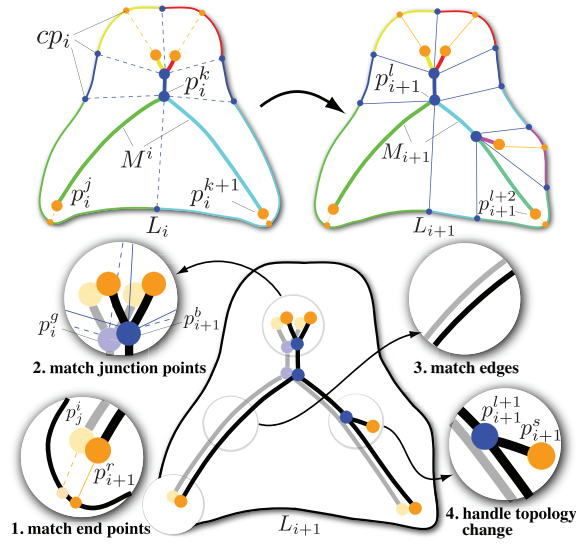Given the above distance and similarity metric, our matching

**Figure 6:** *Illustration of matching algorithm. The top row shows two consecutive slices, $L_i$ and $L_{i+1}$ and their mid-structures, $M_i$ and $M_{i+1}$. The foot points of the end points (orange dots) and junction points (blue dots) are highlighted on the boundaries. Each point in the mid-structure and its foot points are linked through straight lines. The bottom figures illustrates the matching steps 1–4. Note that all the foot points in level $L_i$ have been projected to level $L_{i+1}$. For illustration purpose, we overlap the mid-structure $M_i$ (skeleton with light colors) with $M_{i+1}$ (skeleton with dark colors).*

algorithm can be described as follows (Figure 6). **1.** Match two closest end points. **2.** Match two closest junction points. **3.** Match two edges if their end points are matched pairwise. **4.** Handle topological changes and match remaining edges.

Handling topological changes proceeds as follows. 1) for *Type 1*, a junction point $p_{i+1}^{l+1}$ is introduced (or removed) if a new branch edge $(p_{i+1}^{l+1}, p_{i+1}^s)$ is growing out from (or collapsing onto) an existing edge $(p_i^k, p_i^{k+1})$ that is split to two edges $(p_{i+1}^l, p_{i+1}^{l+1})$ and $(p_{i+1}^{l+1}, p_{i+1}^{l+2})$. We then match $(p_i^k, p_i^{k+1}) \leftrightarrow \left( (p_{i+1}^l, p_{i+1}^{l+1}), (p_{i+1}^{l+1}, p_{i+1}^{l+2}) \right)$. Note that if the new branch edge is growing from an existing junction point, we do nothing. 2) for *Type 2*, there are two unmatched junction points for each graph, e.g. $p_i^j$ and $p_i^{j+1}$ at $M_i$, $p_{i+1}^r$ and $p_{i+1}^{r+1}$ at $M_{i+1}$. They are connected by an edge in their corresponding graph. In the meantime, all their connecting end points are matched pairwisely (see the four end points in the illustrative example of *Type 2* above). It is this configuration that allows us to identify *Type 2* topological change. To handle that, we insert four matching pairs: $p_i^j \leftrightarrow p_{i+1}^r$, $p_i^j \leftrightarrow p_{i+1}^{r+1}$, $p_i^{j+1} \leftrightarrow p_{i+1}^r$, and $p_i^{j+1} \leftrightarrow p_{i+1}^{r+1}$. Note that if a skeleton graph contains only a single node, everything in the successive graph will be mapped to this node. This guarantees

the continuous transition between 1D curve and 2D surface structures of a GSM.

### 6.3. Handling Bifurcations

The aforementioned matching framework works well for level sets with one connected component. It is not sufficient for the case where the number of connected components of the level sets changes at the saddle points of the harmonic function (e.g. the splitting and merging of level sets), for instance, at the basis of the ears of the bunny. We extend the framework to handle the matching at bifurcations as follows.

Let $C_i$ and $C_{i+1}$ be the number of connected components in $L_i$ and $L_{i+1}$, respectively. Assume $C_i < C_{i+1}$ (i.e. splitting). We *project* $cp_i^j$ onto $\partial L_{i+1}$ (If $C_i > C_{i+1}$ (i.e. merging), we project $cq_{i+1}^l$ onto $\partial L_i$). Each projected foot point $cp_{i+1}^{j'}$ is assigned a component index after projection. All the foot points of one node $p_i^j$ are in the same component after projection because of the properties of the harmonic function. We extract sub-graphs from $M_i$ based on the assigned component indices. These sub-graphs are matched with the corresponding components of $M_{i+1}$ using the same algorithm described in Section 6.2.

Let $e_i$ represent the edge $(p_i^j, p_i^{j+1}) \in E_i$ of $M_i$. It splits into two edges in $M_{i+1}$. Assume that $p_i^j$ is matched to $p_{i+1}^l$. We examine the edges adjacent to $p_{i+1}^l$ in $M_{i+1}$, and find out the one whose other end node $p_{i+1}^r$ has not been matched and has the smallest Euclidean distance to $e_i$. We then project $p_{i+1}^r$ onto $e_i$ at $p_i^{r'}$ and construct a partial matching between $(p_i^j, p_i^{r'})$ and $(p_{i+1}^l, p_{i+1}^r)$. We process $p_i^{j+1}$ similarly.
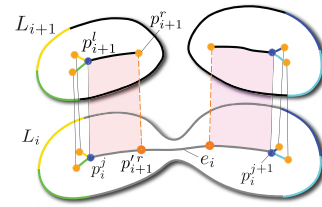


### 7. Results and Discussion

Figure 7 shows results of our framework for a number of graphics, medical, and CAD models. The iterative construction of the GSM allows us to track topological changes of the mid-structures of level sets along the user desired cutting orientation. Different color sheets in Figure 7 represent the evolution of their individual feature components of the mid-structure (the edges of the simplified medial graph). Figure 8 presents a comparison with 1D curve skeletons [ATC*08] and discrete scale axes [MGP10] for a model with tubular and more general regions (see the middle and right columns). Both, the curve skeletons and discrete scale axes are computed using the programs provided by the authors of those papers. This comparison shows that the hybrid structure of the GSM captures the tubular and more general regions of each object as curve and surface elements, while the other
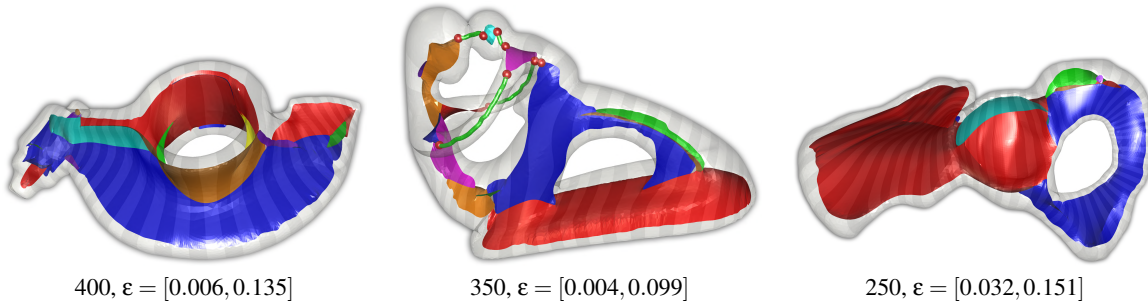
$400, \varepsilon = [0.006, 0.135]$      $350, \varepsilon = [0.004, 0.099]$      $250, \varepsilon = [0.032, 0.151]$

**Figure 7:** *GSMs for rockerarm, fertility and pelvis models. Different GSM sheets are shown in different colors. The sweeping strategy is shown for each model on its boundary. For each GSM, the number of slices and the minimum $\varepsilon$ and maximum $\varepsilon$ are provided below the respective model.*



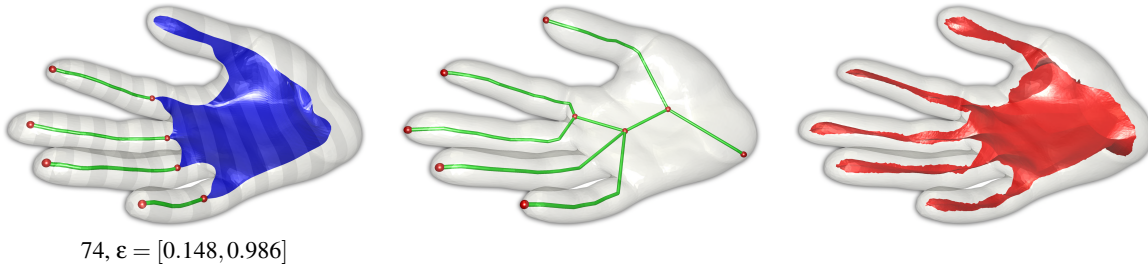$74, \varepsilon = [0.148, 0.986]$

**Figure 8:** *left column: GSM; middle column: 1D curve skeleton; right column: Discrete Scale Axis. Different GSM sheets are shown in different colors. Furthermore, the sweeping strategy is shown on its boundary. The number of slices and the minimum $\varepsilon$ and maximum $\varepsilon$ for the GSM are provided below the respective model. For the curve skeleton, Laplacian constraint scale and positional constraint weight are 2 and 1, respectively. For discrete scale axis, $\delta = 0.01$ and $s = 1.1$.*

two approaches contain only either of the two. The topology of the GSM enables smoothing of sheet boundaries.

The user interaction to compute the harmonic function for the models presented in this paper did not exceed 5 minutes. The remaining pipeline steps to compute the resulting GSM proceeded automatically. To extract one slice and compute its corresponding mid-structure takes about 1 minute in our current implementation. Since this computation can be performed independently per slice, our framework can leverage multi-core computer architectures. We implemented the GSM pipeline on an interlinked Intel Xeon X730 Processor comprised of 32 cores, where GSM computation for the examples shown in this paper did not exceed 20 minutes. In comparison, the representations constructed by global algorithms such as the discrete scale axis [MGP10], the tight co-cone [DG03] or the skeleton computed through mesh contraction [ATC*08] took less than two minutes for the triangle meshes used in this paper. However, the GSM automatically derives the toplogical structure and classifies sheets, whereas given a medial axis computed from existing techniques, significant additional time is required for sheet classification and other post-processing.

Figure 9 shows an example of an object represented with two different triangulations. The input object in Figure 9 (bottom) has a coarser and more irregular triangulation than Figure 9

(top). It can be seen that sharper features lead to distortions of the harmonic function, resulting in larger slicing densities in these regions, e.g., tips of the dolphin fins in Figure 9. The GSM of the coarser mesh still captures the global shape features represented in the GSM of the object with finer mesh. Since the number of slices for the coarser mesh is a quarter of the finer one, the computation time for its GSM is roughly four times faster.

**Limitations:** The GSM pipeline requires the user to specify critical points to compute a harmonic function. An appropriate choice of these points could be challenging for models with more complex geometry and topology. The extremal points of a 1D curve skeleton are given as hints to the user to recommend critical points. Note that the resulting GSM has then a visually similar structure to a medial axis. Another limitation is that slices have to be of genus-0 (i.e. no inner boundaries), which is due to the proposed medial axis computation algorithm for the slices requiring a closed input curve. In addition, sharp features in the input object may not be preserved if the cutting misses the features. Furthermore, the current graph matching cannot handle complex configurations of topological changes. Finally, the current computation is relatively slow due to the slow B-spline root solving. We plan to address these issues in future work.
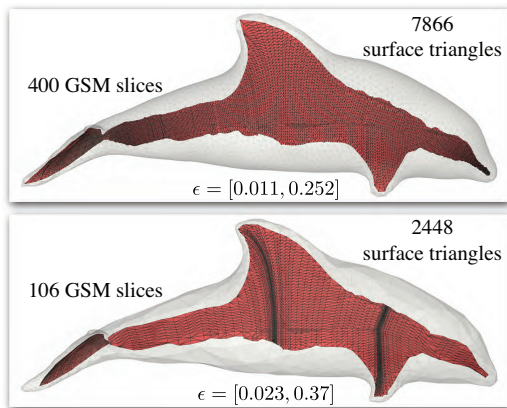
**Figure 9:** *GSMs computed on a uniform vs. coarse feature-aware triangle mesh. Both use one minimum and one maximum. Curved slices created from the harmonic functions are swept from tail to nose and capture overhang regions consistently.*



**Figure 10:** *(a) Cut through a hexahedral mesh, where the mesh layout was determined by the GSM for the respective model; (b) Deformation based on GSM.*

## 8. Applications

In this section we highlight two potential applications for which a GSM can be useful. In the first application, a GSM could be used to generate a semi-structured hexahedral mesh (Figure 10 (a)) by decomposing the input object into simpler subvolumes, where subvolumes correspond to sheets in the GSM. Then, each subvolume is parameterized. Furthermore, the natural parameterization of the GSM could potentially be used for 3D cross field design which is used to generate a hexahedral mesh using a method such as [NRP11]. The proposed GSM pipeline could help in the following way. A desired cutting strategy could be chosen by the user, where the resulting GSM could be used to align hexahedral elements along the chosen sweeping direction.

The second application lets the user deform the object based on the GSM. The consistent topology of the GSM has the potential to produce higher quality deformations compared to other medial and skeleton based shape deformations. Figure 10 (b) shows an example of the model in Figure 8. The fingers could be deformed using skeleton-based deformation, while the palm could be deformed by editing the surface sheet of the GSM through Laplacian mesh editing.

## 9. Conclusions

This paper presents a new hybrid mid-structure called the *Generalized Swept Mid-structure* (GSM), containing curve and surface elements with consistent topology. A pipeline to incrementally construct the GSM of polygonal objects is presented that uses a novel planar mid-structure computation algorithm in conjunction with an algorithm to match two similar 2D mid-structures. The result is a connected structure that the topology of the input surface. The sweeping strategy is
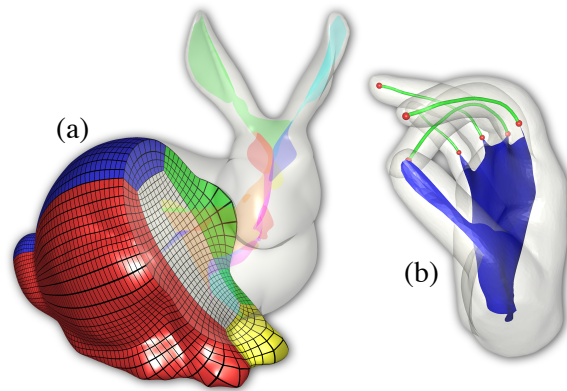
determined by a user who selects a small set of critical points to define a harmonic function that naturally conforms to an object's shape. The GSM is then incrementally constructed by sweeping mid-structures of level sets of the harmonic.

The structure of a GSM is user controlled via the choice of a sweeping strategy and is therefore flexible to adapt appropriately for specific applications. This is not the case for existing skeleton and 3D medial axis algorithms that determine an intrinsic mid-structure. Curve skeletons are more suitable for tube-shaped objects and 3D medial axes are more suitable for objects with more general regions. The hybrid structure of the GSM enables it to be applied for objects consisting of both region types. Existing hybrid skeletonization approaches first compute approximations of 3D medial axes that are then analyzed to differentiate tubular from non-tubular regions. However, those approaches are susceptible to topological issues with the 3D medial axis approximation. We have demonstrated potential GSM applications, such as hexahedral meshing and GSM-based shape deformation.

### References

[AAA*09] AICHHOLZER O., AIGNER W., AURENHAMMER F., HACKL T., JÜTTLER B., RABL M.: Medial axis computation for planar free-form shapes. *Computer-Aided Design 41*, 5 (2009), 339–349.

[ACK01] AMENTA N., CHOI S., KOLLURI R.: The power crust.

In *Proceedings of 6th ACM Symposium on Solid Modeling* (2001), pp. 249–260.

[ATC*08] AU O. K.-C., TAI C.-L., CHU H.-K., COHEN-OR D., LEE T.-Y.: Skeleton extraction by mesh contraction. *ACM Trans. Graph. 27*, 3 (August 2008), 44:1–44:10.

[BAB*08] BIASOTTI S., ATTALI D., BOISSONNAT J., EDELS-BRUNNER H., ELBER G., MORTARA M., BAJA G., SPAGNUOLO M., TANASE M., VELTKAMP R.: Skeletal structures. *Shape Analysis and Structuring* (2008), 145–183.

[CFM*94] CIGNONI P., FLORIANI L. D., MONTANI C., PUPPO E., SCOPIGNO R.: Multiresolution modeling and visualization of volume data based on simplicial complexes. In *VVS '94: Proceedings of the 1994 symposium on Volume visualization* (1994), pp. 19–26.

[cga] CGAL, Computational Geometry Algorithms Library. http://www.cgal.org.

[CKM04] CULVER T., KEYSER J., MANOCHA D.: Exact computation of the medial axis of a polyhedron. *Comput. Aided Geom. Des. 21* (January 2004), 65–98.

[CL04] CHAZAL F., LIEUTIER A.: Stability and homotopy of a subset of the medial axis. In *SM '04: Proceedings of the ninth ACM symposium on Solid modeling and applications* (2004), pp. 243–248.

[Dam08] DAMON J.: Swept regions and surfaces: modeling and volumetric properties. *Theoretical Computer Science* (2008), 66–91.

[DBG*06] DONG S., BREMER P.-T., GARLAND M., PASCUCCI V., HART J. C.: Spectral surface quadrangulation. *ACM Trans. Graph. 25*, 3 (2006), 1057–1066.

[DG03] DEY T. K., GOSWAMI S.: Tight cocone: a water-tight surface reconstructor. In *SM '03: Proceedings of the eighth ACM symposium on Solid modeling and applications* (2003), pp. 127–134.

[DKG05] DONG S., KIRCHER S., GARLAND M.: Harmonic functions for quadrilateral remeshing of arbitrary manifolds. *Computer Aided Geometric Design 22*, 5 (2005), 392–423.

[EG08] ELBER G., GRANDINE T.: Efficient solution to systems of multivariate polynomials using expression trees. In *IEEE International Conference on Shape Modeling and Applications, 2008* (2008), pp. 163–169.

[EK01] ELBER G., KIM M.: Geometric constraint solver using multivariate rational spline functions. In *Proceedings of the sixth ACM symposium on Solid modeling and applications* (2001), ACM New York, NY, USA, pp. 1–10.

[Elb08] ELBER G.: The IRIT modeling environment, version 10.0, 2008.

[FLM03] FOSKEY M., LIN M. C., MANOCHA D.: Efficient computation of a simplified medial axis. In *SM'03: Proceedings of the eighth ACM symposium on Solid modeling and applications* (2003), SM '03, pp. 96–107.

[GDB06] GOSWAMI S., DEY T., BAJAJ C.: Identifying flat and tubular regions of a shape by unstable manifolds. In *Proceedings of the 2006 ACM symposium on Solid and physical modeling* (2006), ACM, pp. 27–37.

[GK03] GIBLIN P., KIMIA B.: On the local form and transitions of symmetry sets, medial axes, and shocks. *International Journal of Computer Vision 54*, 1 (2003), 143–157.

[GT91] GABOW H. N., TARJAN R. E.: Faster scaling algorithms for general graph matching problems. *J. ACM 38* (October 1991), 815–853.

[HTWB11] HUANG J., TONG Y., WEI H., BAO H.: Boundary aligned smooth 3D cross-frame field. *ACM Trans. Graph. 30*, 6 (Dec. 2011), 143:1–143:8.

[Hug00] HUGHES T. J. R.: *The Finite Element Method: Linear Static and Dynamic Finite Element Analysis*. Dover, 2000.

[HXS09] HE Y., XIAO X., SEAH H.-S.: Harmonic 1-form based skeleton extraction from examples. *Graphical Models 71*, 2 (2009), 49 – 62. IEEE International Conference on Shape Modeling and Applications 2008 - SMI '08.

[JBC07] JU T., BAKER M., CHIU W.: Computing a family of skeletons of volumetric models for shape description. *Computer-Aided Design 39*, 5 (2007), 352–360.

[KSK01] KLEIN P. N., SEBASTIAN T. B., KIMIA B. B.: Shape matching using edit-distance: an implementation. In *Proceedings of the 12th annual ACM-SIAM symposium on Discrete algorithms* (2001), SODA '01, pp. 781–790.

[LPRMt02] LÉVY B., PETITJEAN S., RAY N., MAILLO T J.: Least squares conformal maps for automatic texture atlas generation. In *ACM SIGGRAPH conference proceedings* (Jul 2002), ACM, (Ed.).

[LV99] LAZARUS F., VERROUST A.: Level set diagrams of polyhedral objects. In *Proceedings of the fifth ACM symposium on Solid modeling and applications* (1999), ACM, pp. 130–140.

[MC10] MARTIN T., COHEN E.: Volumetric parameterization of complex objects by respecting multiple materials. *Comput. Graph. 34* (June 2010), 187–197.

[MCK08] MARTIN T., COHEN E., KIRBY M.: Volumetric parameterization and trivariate B-spline fitting using harmonic functions. In *SPM '08: Proceedings of the 2008 ACM symposium on Solid and physical modeling* (2008), pp. 269–280.

[MGP10] MIKLOS B., GIESEN J., PAULY M.: Discrete scale axis representations for 3D geometry. *ACM Trans. Graph. 29*, 4 (July 2010), 101:1–101:10.

[NGH04] NI X., GARLAND M., HART J. C.: Fair Morse functions for extracting the topological structure of a surface mesh. In *Proc. SIGGRAPH* (2004).

[NRP11] NIESER M., REITEBUCH U., POLTHIER K.: CUBE-COVER - parameterization of 3D volumes. *Computer Graphics Forum 30*, 5 (2011), 1397–1406.

[RG03] RAMANATHAN M., GURUMOORTHY B.: Constructing medial axis transform of planar domains with curved boundaries. *Computer-Aided Design 35*, 7 (2003), 619–632.

[SFM05] SUD A., FOSKEY M., MANOCHA D.: Homotopy-preserving medial axis simplification. In *Proceedings of the 2005 ACM symposium on Solid and physical modeling* (2005), ACM, pp. 39–50.

[Si05] SI H.: Tetgen: A quality tetrahedral mesh generator and three-dimensional delaunay triangulator.

[SP08] SIDDIQI K., PIZER S.: *Medial representations: mathematics, algorithms and applications*. Springer Verlag, 2008.

[SSDZ98] SIDDIQI K., SHOKOUFANDEH A., DICKINSON S. J., ZUCKER S. W.: Shock graphs and shape matching. In *Proceedings of the Sixth International Conference on Computer Vision* (1998), ICCV '98, IEEE Computer Society, pp. 222–229.

[SSS06] SCHREINER J., SCHEIDEGGER C., SILVA C.: High-quality extraction of isosurfaces from regular and irregular grids. *IEEE Transactions on Visualization and Computer Graphics 12*, 5 (2006), 1205–1212.